International Journal of Minerals, Metallurgy and Materials
Volume 25, Number 4, April 2018, Page 429
https://doi.org/10.1007/s12613-018-1588-5

Aging behavior of a copper-bearing high-strength low-carbon steel

Babak Shahriari, Reza Vafaei, Ehsan Mohammad Sharifi, and Khosro Farmanesh

Department of Materials Engineering, Malek Ashtar University of Technology, P.O. Box 83145/115, Shahin Shahr, Isfahan, Iran
(Received: 10 June 2017; revised: 7 October 2017; accepted: 10 October 2017)

Abstract: The effects of aging temperature and time on the hardness and impact toughness of a copper-bearing high-strength low-carbon steel were investigated. The hardness of the aged samples reached maxima after 1 h and 5 h of aging at 500 and 450°C, respectively; this increase in hardness was followed by a decrease in hardness until a temperature of 700°C, at which secondary hardening was observed. The impact toughness of the aged steel was found to be higher for 5 h of aging. Transmission electron microscopy confirmed the presence of carbide and copper precipitates; also, the secondary hardening could be the result of the transformation of austenite (formed in the aging treatment) to martensite. Differential scanning calorimetry of the steel was performed to better understand the precipitation behavior. The results revealed that the precipitation of the steel exhibited two significant stages of copper precipitate nucleation and coarsening of the precipitates, with corresponding activation energies of 49 and 238 kJ·mol^{-1}, respectively.

Keywords: aging treatment; BA-160 steel; differential scanning calorimetry; precipitation

1. Introduction

BA-160 steel is a newly designed low-carbon bainitic–martensitic steel that combines the attractive properties of a minimum yield stress of 1100 MPa at room temperature and a high impact toughness of 108 J at −40°C [1]. The very low-carbon content of BA-160 steel, in conjunction with strong carbide-forming elements such as V, Mo, and Cr, can lead to the elimination of cementite, which forms microvoid nucleation sites that degrade the toughness of the steel. Strengthening can be achieved via the simultaneous precipitation of M_2C carbides and Cu precipitates.

Numerous investigations on Cu-strengthened ship hull steels such as HSLA-80 and HSLA-100 steels have been reported [2–4]. Concerning the alloying content, the latter steel provides the most important basis for the design of BA-160 steel. However, the contribution of Cu and carbide precipitations to strength is more remarkable for the BA-160 steel than for the HSLA-100 steel [1,5]. The very high potential of precipitation hardening, in addition to the greater hardenability of the steel resulting from the higher alloying content (greater than 12wt%), makes the effects of other strengthening mechanisms less perceptible.

Differential scanning calorimetry (DSC) is a well-developed method for studying a wide range of phase transformations [6–8], including Cu precipitation in steels. Ren *et al.* [9] studied several austenitic antibacterial stainless steels with Cu concentrations ranging from 3.8wt% to 5.0wt% via DSC analysis. They observed two stages of precipitation in the steel by DSC analysis: clustering of Cu-rich phases and dissolution and/or coarsening of the formerly formed precipitates. Maruyama *et al*. [10] used DSC analysis to explore the precipitation behavior of low-alloy ferritic and martensitic steels. Their investigation revealed that the DSC curves of ferritic steels displayed three exothermic peaks, which were converted into two peaks in the curves of martensitic steels.

Few investigations on the aging of BA-160 steel have been reported; this knowledge gap can be partially filled using DSC analysis. In the present work, the aging behavior of BA-160 steel was investigated, and the kinetics of precipitation was studied using DSC analysis.

2. Experimental

The experimental steel was prepared by vacuum melting of the steel with a very low level of carbon, impurities, and

Corresponding author: Ehsan Mohammad Sharifi E-mail address: ehsan_sharifi_2000@yahoo.com

tramp elements and with high-purity alloying additions to yield 5 kg of BA-160 steel. The chemical analysis of the cast steel was measured by optical emission spectroscopy; the results are summarized in Table 1. The ingot was homogenized at 1200°C for 2 h and then subjected to hot forging at 1100°C to obtain the final thickness of 37 mm after more than 50% reduction. The forged metal was subsequently rolled at 900°C to a final thickness of 12 mm.

Table 1. Chemical analysis results for the experimental BA-160 steel wt%

C	P	S	Cr	Mo	Ni	V	Ti	Mn	Al	Cu	O	N
0.04	0.006	0.005	2.10	0.65	6.67	0.12	0.03	0.11	0.009	3.63	0.002	0.003

2.1. Aging treatments

Samples were cut from the as-rolled BA-160 steel plate and subjected to a solution annealing heat treatment at 900°C for 1 h; this treatment was followed by water quenching. Aging treatments were subsequently conducted for different times and at different temperatures in an appropriate hot-air circulation furnace. The aging temperatures were varied from 400 to 700°C in increments of 50°C for 1 and 5 h. Three specimens for each temperature–time condition were aged. After the aging treatment, the samples were cooled in air and at least 1 mm of the samples was removed from the surfaces to ensure elimination of the probable decarburized layer.

2.2. Differential scanning calorimetry

For DSC analysis, a piece of steel was solution annealed as previously mentioned and cut into discs with a diameter of 5 mm and a thickness of 0.5 mm. DSC analysis of the precipitation behavior was conducted using a Netzsch STA 449F3 thermal analyzer; the specimens were heated under a nitrogen atmosphere at a heating rate of 15, 20, or 25°C·min^{-1}. Each experiment at each specific heating rate was repeated four times to minimize the related errors. Prior to DSC measurements, the zero-line of the apparatus with empty crucibles was determined at each heating rate and was subtracted from the measured heat-flow curves to eliminate the thermal variations resulting from the characteristics of the apparatus itself. Baseline correction was performed using a second-order derivative technique followed by peak finding through a local maximum method. Finally, the Kissinger method [11] was used to evaluate the kinetics of precipitation in the BA-160 steel.

2.3. Evaluation tests

Charpy V-notch (CVN) specimens were machined according to the standard specified in ASTM A370. The Charpy tests were performed at −20°C. The fracture surfaces of the broken specimens after impact were observed by scanning electron microscopy (SEM, Zeiss EVO 50 EP). Also, field-emission gun-scanning electron microscopy (FEG-SEM, Tescan Mira 3-XMU) was used to characterize and examine the resulting microstructures. A JEOL 3200FS-HR field-emission transmission electron microscope operating at 300 kV was used for bright-field and dark-field imaging and for energy-dispersive spectroscopy (EDS) analysis. The transmission electron microscopy (TEM) samples were discs with a diameter of 3 mm; they were punched from the steel slices and thinned by grinding to 100-μm thick. Final thinning was carried out on a Struers TenuPol-5 electropolisher using a solution of 15vol% perchloric acid in methanol at −30°C to achieve electron transparency.

The critical temperatures of the steel were determined using a Bahr DIL-805A/D dilatometer at a protective atmosphere of pure argon. The samples for dilatometry analysis were cylindrical, with a height of 10 or 4 mm. During the thermal cycle of dilatometry, the experimental steel was heated at a rate of 5°C·s^{-1} and austenitized at 900°C for 10 min; it was then cooled at a cooling rate of 1°C·s^{-1}. The standard deviation of the measurements was ±3°C.

3. Results

3.1. Characterization and evaluation after aging

Fig. 1(a) shows the microstructure of the as-rolled BA-160 steel; it consisted of a mixture of martensite and bainite. Fig. 1(b) is an SEM morphology image of the steel after the solution annealing treatment and quenching, showing a martensitic microstructure. Fig. 2(a) is a typical TEM bright-field image of the BA-160 steel aged at 550°C for 5 h. It shows a microstructure with numerous precipitates, some of which are indicated by arrows. The precipitates had a spheroidal shape with a typical diameter of 16 nm. Fig. 2(b) is the corresponding dark-field image in which some of the precipitates are more clearly observed. Fig. 2(c) is the selected-area diffraction (SAD) pattern of one of the precipitates. The key diagram corresponding to Fig. 2(c) is shown in Fig. 2(d); it shows ε-Cu and $M_{23}C_6$ precipitates, along with α-Fe (ferritic bainite or martensite).

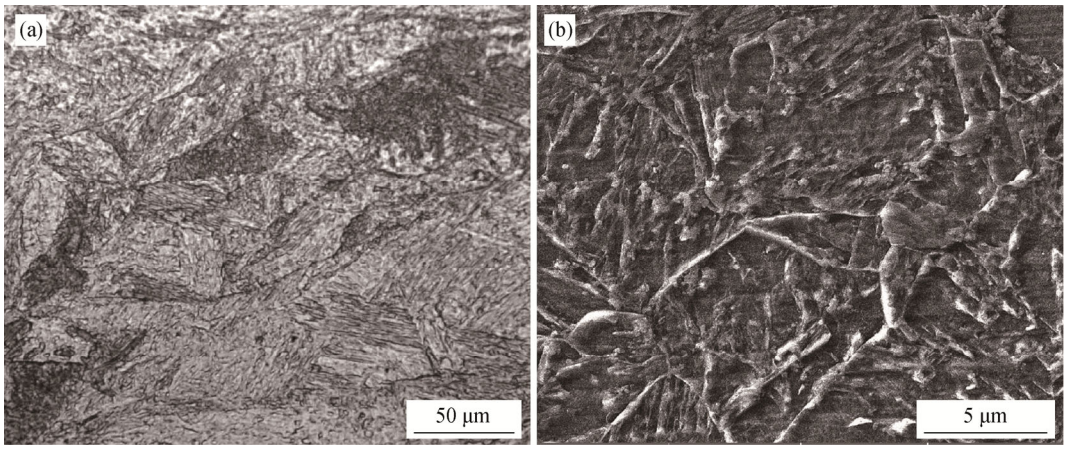

Fig. 1. Microstructures of BA-160 steel: (a) optical micrograph of a specimen in the as-rolled condition; (b) an SEM image after the solution annealing treatment and quenching.

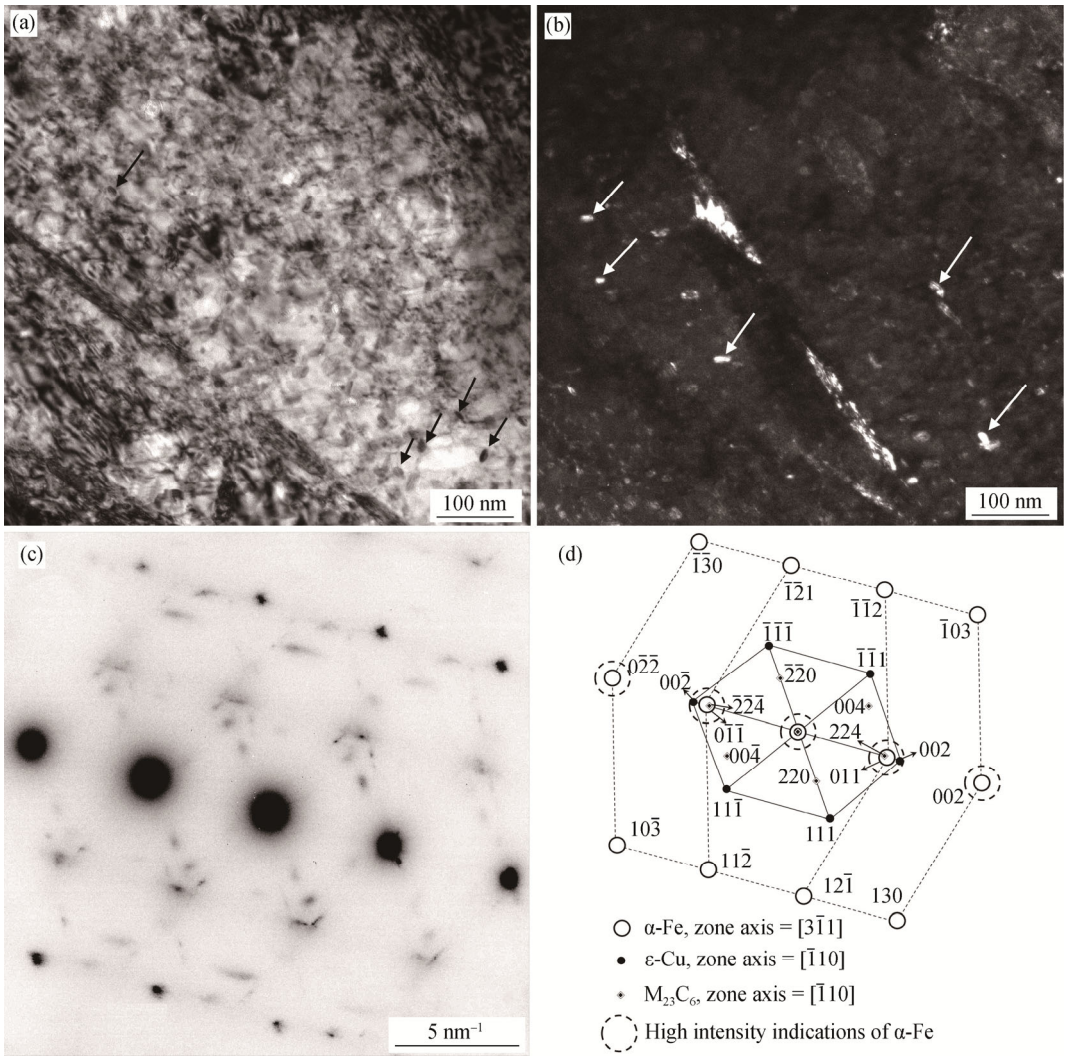

Fig. 2. TEM microstructures of the BA-160 steel after aging at 550°C for 1 h, including nanometric precipitates: (a) bright-field image; (b) the corresponding dark-field image, in which the precipitates are indicated by arrows; (c) SAD pattern of one of the precipitates; (d) the key diagram corresponding to Fig. 2(c).

The hardness values of the specimens aged at different times and temperatures are shown in Fig. 3. For the specimens aged for 5 h, the hardness tended to increase as the aging temperature was increased to 450°C. However, a fairly sharp decrease in hardness was observed in samples aged for 5 h at temperatures between 450 and 650°C. The samples aged for 1 h showed a rather constant hardness between 450 and 550°C, with a weak maximum at 500°C. All aging temperatures used for 1 h experiments resulted in higher hardness values except 400 and 450°C. Furthermore, the hardness variations shown in Fig. 3 reveal that, after the peak hardness was reached, the hardness of the steel decreased as the temperature was increased to 650°C; at 700°C, secondary hardening occurred in both the 1-h- and 5-h-aged samples.

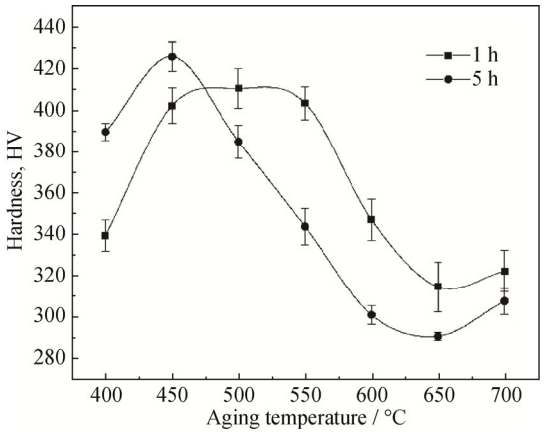

Fig. 3. Variations of hardness versus temperature during the aging of the BA-160 steel for aging times of 1 h and 5 h.

Variations of the CVN impact energy of the BA-160 steel under various aging conditions are shown in Fig. 4. The higher impact energies in Fig. 4 correspond well with the lower hardness values in Fig. 3 and vice versa. Moreover, Fig. 4 shows that, at temperatures greater than 450°C, the impact energies of the steel aged for 5 h were higher than the CVN energies for 1-h-aged samples.

Fig. 5 displays fractographs of the broken samples aged at 450 and 600°C for 1 and 5 h, after the impact tests. The fracture surface of the samples aged at 450°C (Figs. 5(a) and 5(c)) show a typical brittle fracture with a river-pattern-type cleavage and a quasi-cleavage appearance. The samples aged at 600°C (Figs. 5(b) and 5(d)) show dimples on the fracture surface—a typical characteristic of ductile fracture.

3.2. DSC analysis and kinetics of precipitation

DSC analysis of the BA-160 steel was performed at three heating rates (15, 20, and 25°C·min^{-1}), with each run being repeated four times. Fig. 6 shows typical thermograms obtained at different heating rates. Three peaks were observed, as shown in Fig. 6, two of which (P_I and P_{II}) were exothermic within the temperature ranges of 299–325°C and 494–506°C, respectively; the other (P_{III}) was an endothermic peak at approximately 727°C. A shift of peaks to higher temperatures as a result of the increase in heating rate reveals the thermally activated nature of the involved phase transformations.

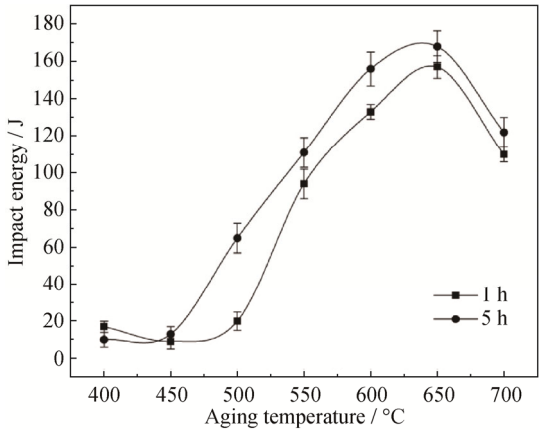

Fig. 4. Measured impact energies at −20°C of the BA-160 steel aged at different temperatures for aging times of 1 h and 5 h.

The activation energies of reactions were found from the peak temperatures of the thermo grams. According to the Starink analysis [12], the Kissinger technique is one of the best known isoconversion methods for the determination of activation energy; it is expressed as

$$\ln\left[\frac{\beta}{T_p^2}\right] = \ln\left[\frac{AR}{E}\right] - \frac{E}{R}\cdot\frac{1}{T_p} \quad (1)$$

where β is the heating rate, T_p is the temperature at the reaction peak, R is the gas constant, E denotes the activation energy for the reaction involved, and A is the pre-exponential factor. Thus, the activation energy of the reactions can be derived from the slope of a plot of $\ln(\beta/T_p^2)$ versus $(1/T_p)$, which is $(-E/R)$. The plots corresponding to peaks I and II of different DSC curves are shown in Fig. 7. The effective activation energies for peaks I and II were calculated to be 49 and 238 kJ·mol^{-1}, respectively.

4. Discussion

4.1. Aging treatments

SAD analysis of the precipitates showed that ε-Cu and $M_{23}C_6$ carbides were simultaneously present in the precipitate particles. High-resolution TEM studies have shown that Cu precipitates during gradual growth undergo a series

of transformations from bcc Cu to 9R; a more stable structure of 3R forms, and fcc ε-Cu precipitates are finally developed [13–16]. After reaching a critical size of 12 nm, Cu precipitates have been shown to exhibit an fcc structure [17].

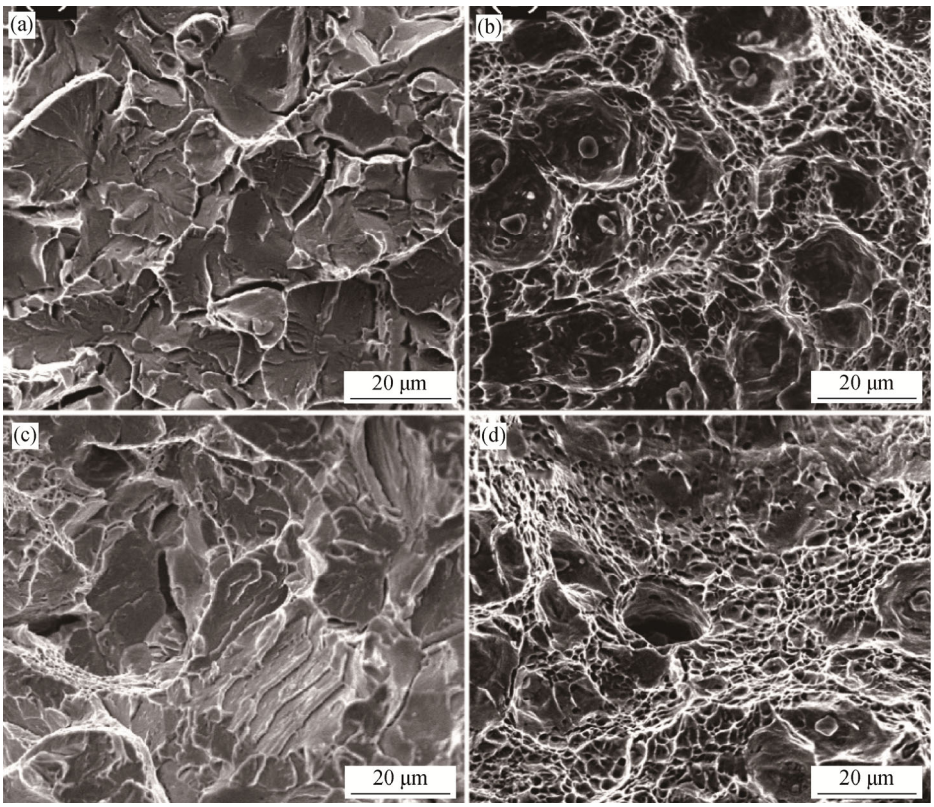

Fig. 5. Fractographs of the broken Charpy impact samples aged at temperatures of (a) 450°C for 1 h, (b) 600°C for 1 h, (c) 450°C for 5 h, and (d) 600°C for 5 h.

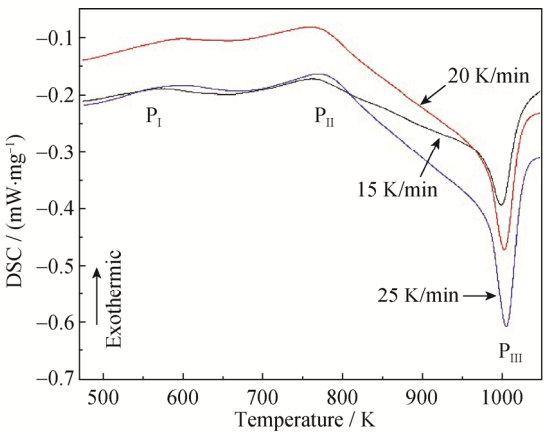

Fig. 6. Typical DSC curves of the BA-160 steel at different heating rates.

Numerous investigations have shown that the orientation relationship (OR) between the fcc Cu precipitates and the α-Fe matrix is of the Kurdjumov–Sachs (K–S) type [18–19]. The K–S OR is represented as $\{111\}_{fcc}//\{110\}_{bcc}$ and $\langle\bar{1}10\rangle_{fcc}//\langle\bar{1}11\rangle_{bcc}$, where braces and angled brackets denote crystallographic families of planes and directions, respectively. However, the key diagram in Fig. 2(d) shows that the (011) planes of α-Fe nearly coincide with the (002) planes of ε-Cu and their respective zone axes, such that the $[3\bar{1}1]$ and $[\bar{1}10]$ are parallel. Comparing this relationship with the K–S as well as four other known ORs related to the interfaces formed between bcc and fcc structures—specifically, the Bain, Nishiyama and Wasserman (N–W), Greninger and Troiano (G–T), and the Pitsch ORs [20]—reveals that the current OR may not be attributable to one of these ORs.

The EDS analysis results also indicate that the precipitates were enriched with Cu and with carbide-forming elements such as Cr. These findings are consistent with the results reported by Mulholland *et al*. [5] showing that carbides select Cu precipitates as nucleation sites.

Fig. 8 is a graphical representation of a set of data derived from the literature, showing the isothermal aging behavior of the BA-160 steel at 450°C with different aging times; the compositions of the steels are also given in Table 2. Notably, the results attributed to Mulholland *et al*. [5] were regenerated from their work concerned with the measurement of yield stress versus aging time. In the present

work, the results of Mulholland *et al*. have been converted to hardness versus aging time using the relationship proposed by Saha *et al*. [21]. Both the Saha [1] and Mulholland results show that the maximum hardness of the BA-160 steel aged at 450°C was realized after 5 h of aging. Thus, aging at 450°C for 1 h could not impart the maximum possible hardness to the steel, whereas it was reached through aging at 450°C for 5 h. A similar trend was expected for the aging treatment at 400°C because aging at lower temperatures should result in a higher peak hardness; however, for the peak condition to be realized, a much longer heating time is required [22].

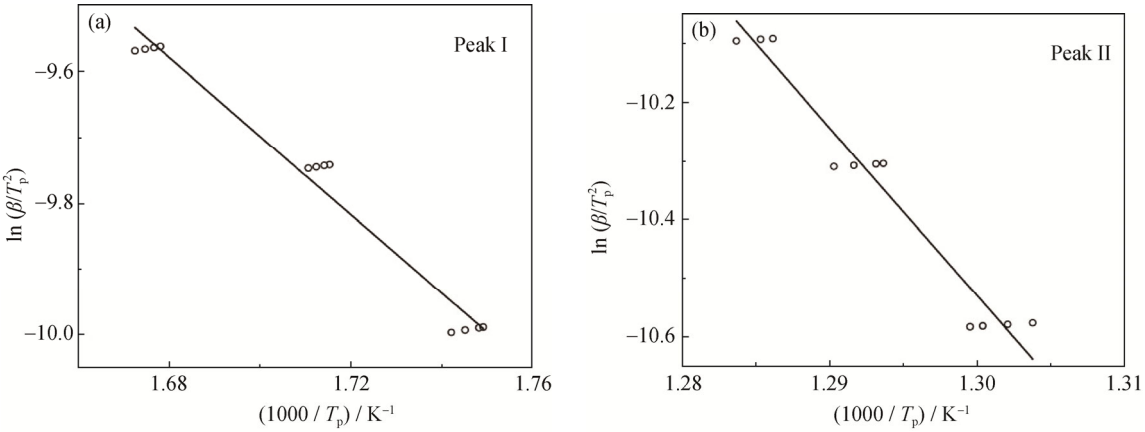

Fig. 7. Plots for the calculation of the activation energy based on (a) peak I and (b) peak II of the DSC curves.

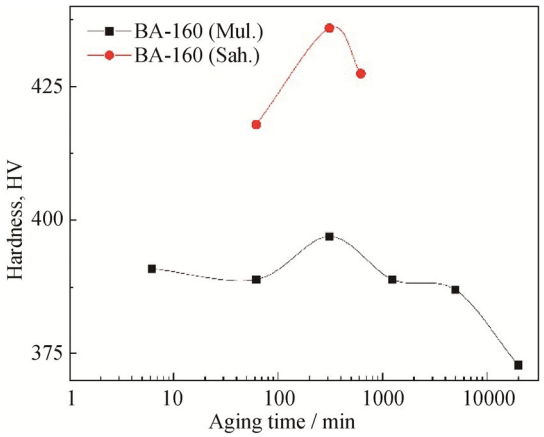

Fig. 8. Variations of hardness versus time during the aging of the BA-160 steel at 450°C based on the results reported by Saha *et al.* [1] and Mulholland *et al.* [5].

Table 2. Chemical compositions of BA-160 steels studied by different authors wt%

Author	C	Cr	Mo	Cu	Ni	V	Ref.
Saha *et al.*	0.040	1.78	0.58	3.64	6.61	0.11	[1]
Mulholland *et al.*	0.060	1.89	0.50	3.33	6.42	—	[5]

The relationship between the time and the temperature of a heat treatment involving diffusion-controlled processes can be represented using the Hollomon–Jaffe (HJ) parameter, which is defined as $P_{HJ} = T[C + \ln t]$, where T is the absolute temperature (K) and t is the aging time (min). A certain value of this parameter indicates a fixed level of properties such as hardness/strength in heat treatment, for which the constant C is determined. The constant is commonly on the order of 20; here, according to the work of Saha *et al*., it is considered to be 18 [1].

After 5 h at 450°C, the BA-160 steel started to become overaged; according to the HJ parameter, this stage commenced earlier at higher aging temperatures. Thus, at temperatures higher than 450°C, the samples with 1 h of aging, because of less overaging, would show a higher hardness than the samples aged for 5 h.

At peak hardness, the maximum density of coherent bcc Cu precipitates is realized [23]. The precipitates effectively hinder the movement of dislocations, leading to an increase in hardness or strength; however, a degradation of the toughness of the alloy can simultaneously lead to an inverse behavior in the trends of hardness and CVN energy. Many investigators have considered the coarsening of Cu precipitates as the main factor responsible for the decrease in hardness during overaging of Cu-bearing steels at high temperatures [22,24–26]. Mujahid *et al*. [24] indicated that, after the aging of HSLA-100 steel at low aging temperatures, the matrix of the steel was composed of some lath martensite with a similar dislocation density compared to that of the initial sample before aging. However, the increase in aging temperature (after peak hardness) could lead to the sequential recovery of lath martensite and coarsening of precipitates from the bcc spherical shape to fcc ε-Cu and rod-like particles. Hamano [27] has argued that the decrease of toughness and ductility in precipitation-hardened alloys ori-

ginates from the inhomogeneous deformation and the increased stress concentration imposed by the coherency of precipitates. However, the simultaneous presence of incoherent precipitates causing precipitation hardening and coherent precipitates leads to enhanced toughness and ductility. Coherent precipitates concentrate the slip of dislocations in the limited slip bands because they are easily cut by dislocations. Thus, the high density of coherent precipitates results in premature cracking and in a decrease of toughness, which can be alleviated by overaging. According to the discussion of Skoufari-Themistou *et al*. [28] regarding the impact toughness of an experimental Cu-strengthened steel, incoherent deformable Cu precipitates dampen the dynamic energy of cracks and enhance impact toughness.

One of the acceptable combinations of hardness and impact toughness of the BA-160 steel, according to Figs. 3 and 4, could be attained by aging at 550°C for 1 h. These conditions result in a CVN impact energy of 94 J and a hardness of HV 404; the equivalent yield stress, according to the relation proposed by Saha *et al*., is 1155 MPa. The impact toughness result is suitable for many naval applications, as indicated in the standard specification covering HSLA-100 steel, which is 90 J at −18°C [29]. Prolonging the aging treatment to 5 h could result in a 15% decrease in hardness (i.e., a hardness of HV 344, which is equivalent to a yield stress of 950 MPa) and a 17% increase in impact energy (110 J). However, aging at 600°C for 1 h could reduce the hardness to HV 347 (with the equivalent yield stress of 960 MPa) and increases the CVN energy to 133 J; meanwhile, the hardness and impact energy after 5 h of aging at this temperature are HV 301 (equivalent yield stress of 805 MPa) and 156 J, respectively; these values are unacceptable because of the low yield stress. Comparatively, the hardness of the BA-160 steel in the current study was increased by aging at 550°C for 1 h, and the impact energy based on the results of Saha *et al*. was decreased (approximately HV 365 and 125 J, respectively) [1].

The dilatometry curve of the BA-160 steel at a heating rate of $5°C·s^{-1}$ and a cooling rate of $1°C·s^{-1}$, as represented in Fig. 9, shows that the temperature of 700°C lies in the austenite–ferrite intercritical region. Application of the lever rule for the dilatometry curve at 700°C indicates that the amount of austenite phase was greater than 1.5vol%; thus, it could be transformed to martensite during cooling. The formation of the new untempered martensite during cooling from the aging temperature could lead to an increase in hardness. The onset of the change in the slopes of the 1-h and 5-h aging curves, as shown in Fig. 3, for temperatures lower than 650°C indicates that the formation of austenite through the aging treatment and the subsequent transformation to martensite during cooling began at temperatures lower than A_{C1}. This behavior might be due to minor inhomogeneities in the distribution of the alloying elements, resulting in a lower A_{C1} in some areas. These areas could be transformed to austenite at relatively lower aging temperatures and, subsequently, into martensite during the cooling stage.

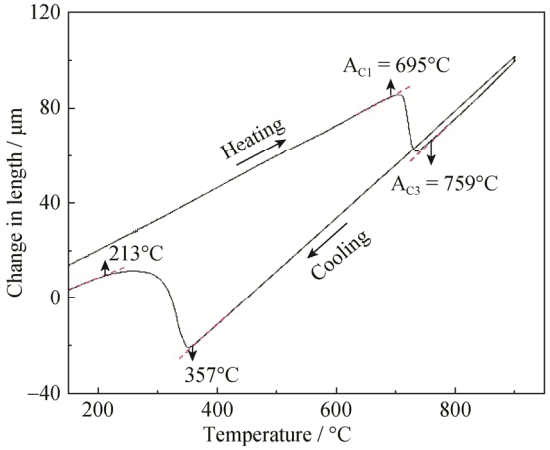

Fig. 9. Dilatation curve versus temperature, showing the ferrite-to-austenite start and finish temperatures (A_{C1} and A_{C3}) and the austenite decomposition start and finish temperatures.

Fig. 10 provides confirmation of this austenite-to-martensite transformation. Fig. 10(a) shows a TEM bright-field image of the bainite laths of the BA-160 steel after aging at 600°C for 5 h. The arrow indicates a region of interlath phase with a different morphology relative to that of the other bainite laths. EDS analysis results for the points shown in Fig. 10(a) are presented in Table 3. The interlath phase (point 2), as compared with points 1 and 3, which are the two surrounding laths, was richer in austenite stabilizer elements (Ni, Mn, and Cu). The total amount of austenite stabilizers was 6.9wt%, 9.2wt%, and 7wt% for points 1, 2, and 3, respectively. This result reveals that the interlath phase exhibited higher resistance to transformation to bainite and could retain the austenite phase commonly observed between laths of martensite or bainite. However, analysis of the SAD pattern of this region (Fig. 10(b)) reveals that the phase corresponding to point 2 was α-Fe, which can be attributed to the martensite phase. In fact, the morphology of the interlath phase of Fig. 10(a) was very similar to that of the retained austenite after cooling; that is, it could form during the aging treatment and transform to martensite during subsequent cooling. Li *et al*. [30] have reported similar morphologies of retained austenite with widths of 30–40 nm, describing them as ultra-fine film-like

retained austenite. They considered that these films of retained austenite resulted from carbon partitioning into the retained austenite after the formation of the supersaturated lower-bainitic ferrite.

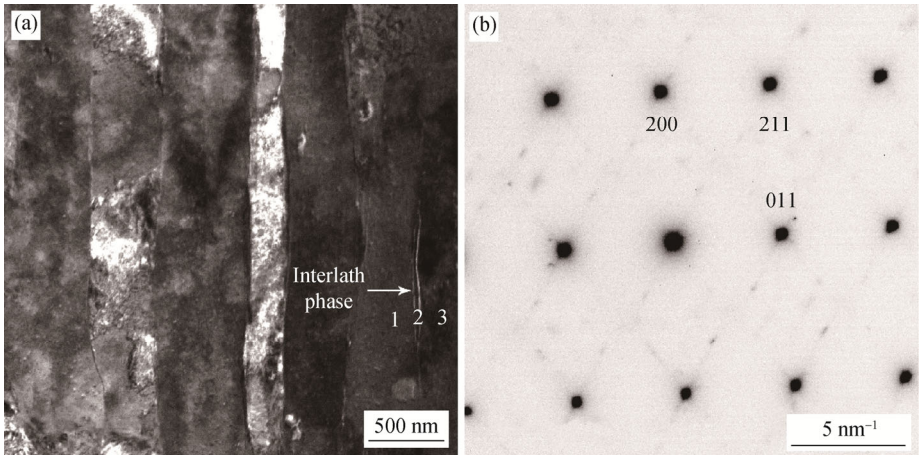

Fig. 10. TEM bright-field image showing a region of the interlath phase in the BA-160 steel aged at 600°C for 5 h (a) and SAD pattern of the interlath phase related to α-Fe (b).

Table 3. EDS chemical analysis results corresponding to the digit positions in Fig. 10(a) wt%

Position	Ni	Cu	Cr	Mo	V	Mn
Point 1	5.18	1.78	2.66	0.69	0.15	0.00
Point 2	5.98	3.08	2.17	0.58	0.22	0.16
Point 3	4.80	2.09	1.84	1.13	0.49	0.00

Maruyama *et al*. [10] investigated martensitic Mn-, Ni-, and Cu-bearing steels using atom probe analysis and showed that Mn and Ni segregated around Cu precipitates. The segregations were detected after 30 min of isothermal aging at 550°C, and the amount of Mn at the interface was approximately 8.1at%. Isheim *et al*. [31] confirmed these results in a recent atom probe tomography study. They reported that the segregations of Ni and Mn at the interface increased with increasing aging time, eventually developing into a distinct layer enveloping the precipitates. Moreover, their results implied that the enriched layer, which did not exceed 2 nm, could have twice or more the Ni and Mn contents of the matrix. Therefore, we concluded that interparticle areas might have lower amounts of austenite stabilizers such as Ni, as evident from the results in Table 3. In addition, the three points had lower Ni contents relative to the total Ni content of the steel. Thus, the amount of Ni required for effective stabilization of austenite based on the design of Saha *et al*. [21] was reduced, which could lead to the transformation to martensite during the subsequent cooling.

Comparable cases of secondary hardening have been reported in other investigations involving HSLA-100 steel [24,32]. According to the discussions reported in these studies, these findings are attributable to the transformation of the austenite already formed during aging to martensite during cooling. Similar to precipitation hardening, new martensite formation leads to hardening and reduces the impact toughness, as evident in Fig. 4.

Secondary hardening of the BA-160 steel, observed from Fig. 3 and the results of Fig. 10, reveals that at least partial transformation to martensite could occur for the austenite phase at aging temperatures of 600°C and above.

4.2. Differential scanning calorimetry

The two exothermic peaks (P_I and P_{II}) detected by DSC analyses could be related to Cu precipitation, and the endothermic peak (P_{III}) was due to the transformation of martensite to austenite. The calculated activation energies for coarsening of clusters with regard to peaks I and II are consistent with the values reported in the literature, which are 54.4 and 244 kJ·mol^{-1}, respectively [10].

Maruyama *et al*. [10] also detected two similar peaks in the DSC thermo gram of a Cu-bearing martensitic steel. Their results showed that peaks I and II occurred at approximately 327 and 527°C, respectively. They attributed the first peak to clustering and the second one to coarsening during the Cu precipitation process. The activation energies of the peaks in their work were also similar to the values reported in the present study. Ren *et al*. [9] investigated the Cu precipitation in an austenitic antibacterial stainless steel containing carbide-forming elements such as Cr and Mo, similar to the BA-160 steel. They reported three sequential peaks, including an exothermic peak and an endothermic peak associated with a weak exothermic peak. They re-

ported an overall activation energy of 181 kJ·mol^{-1} for the Cu precipitation in the steel; this value is substantially different from the activation energy of Cu diffusion in austenite (306.2 kJ·mol^{-1}) [33].

5. Conclusions

The aging behavior of the low-carbon Cu-bearing steel was investigated at different temperatures and times. In addition, DSC analysis of the steel was used to characterize the kinetic behavior of precipitation in the steel. Accordingly, the following conclusions can be drawn:

(1) Analysis of SAD patterns of the nanometric precipitates showed that $M_{23}C_6$ and fcc Cu phases were present in the precipitates.

(2) The peak hardness values of aged samples occurred at temperatures of 500°C for 1 h and 450°C for 5 h. Aged samples showed a reduction in hardness at temperatures greater than the peak up to 650°C; at higher temperatures, secondary hardening was observed.

(3) The results showed that austenite was formed at aging temperatures of approximately 600°C and above; this austenite was not sufficiently stable through subsequent cooling and was transformed into martensite, eventually leading to a secondary hardening at 700°C.

(4) The CVN impact energy decreased with increasing hardness, which was achieved through aging for 5 h at temperatures greater than 450°C; the observed increases in impact energies were greater than those observed for the samples aged for 1 h.

(5) DSC analysis of the BA-160 steel showed one endothermic and two exothermic peaks; the exothermic peaks were due to the precipitation process. The first exothermic peak was well attributable to the nucleation of Cu precipitates, whereas the second peak was associated with the diffusion of Cu in α-Fe required for the coarsening of the precipitates.

References

[1] A. Saha, J. Jung, and G.B. Olson, Prototype evaluation of transformation toughened blast resistant naval hull steels: Part II, *J. Comput. Aided Mater. Des.*, 14(2007), No. 2, p. 201.

[2] Y. Nie, C.J. Shang, X. Song, Y. You, C. Li, and X.L. He, Properties and homogeneity of 550-MPa grade TMCP steel for ship hull, *Int. J. Miner. Metall. Mater.*, 17(2010), No. 2, p. 179.

[3] A.N. Chiaramonti, J.W. Sowards, D.K. Schreiber, and J.R. Fekete, Understanding the high-temperature mechanical properties of A710 (HSLA-80) steel with use of complementary atom probe tomography and electron microscopy, *Microsc. Microanal.*, 20(2014), Suppl. 3, p. 954.

[4] G.H. Majzoobi, A.H. Mahmoudi, and S. Moradi, Ductile to brittle failure transition of HSLA-100 steel at high strain rates and subzero temperatures, *Eng. Fract. Mech.*, 158(2016), p. 179.

[5] M.D. Mulholland and D.N. Seidman, Nanoscale co-precipitation and mechanical properties of a high-strength low-carbon steel, *Acta Mater.*, 59(2011), No. 5, p. 1881.

[6] F. Khodabakhshi and M. Kazeminezhad, Differential scanning calorimetry study of constrained groove pressed low carbon steel: recovery, recrystallisation and ferrite to austenite phase transformation, *Mater. Sci. Technol.*, 30(2014), No. 7, p. 765.

[7] Z.B. Han, J.H. Liu, Y. He, K.W. Li, Y.L. Ji, and J. Liu, Determination of the liquidus and solidus temperatures of Fe-CrAl stainless steel, *Int. J. Miner. Metall. Mater.*, 22(2015), No. 11, p. 1141.

[8] E. Wielgosz and T. Kargul, Differential scanning calorimetry study of peritectic steel grades, *J. Therm. Anal. Calorim.*, 119(2015), No. 3, p. 1547.

[9] L. Ren, L. Nan, and K. Yang, Study of copper precipitation behavior in a Cu-bearing austenitic antibacterial stainless steel, *Mater. Des.*, 32(2011), No. 4, p. 2374.

[10] N. Maruyama, M. Sugiyama, T. Hara, and H. Tamehiro, Precipitation and phase transformation of copper particles in low alloy ferritic and martensitic steels, *Mater. Trans., JIM*, 40(1999), No. 4, p. 268.

[11] R.L. Blaine and H.E. Kissinger, Homer kissinger and the kissinger equation, *Thermochim. Acta*, 540(2012), p. 1.

[12] M.J. Starink, The determination of activation energy from linear heating rate experiments: a comparison of the accuracy of isoconversion methods, *Thermochim. Acta*, 404(2003), No. 1-2, p. 163.

[13] R. Monzen, M. Iguchi, and M.L. Jenkins, Structural changes of 9R copper precipitates in an aged Fe-Cu alloy, *Philos. Mag. Lett.*, 80(2000), No. 3, p. 137.

[14] R. Monzen, M.L. Jenkins, and A.P. Sutton, The bcc-to-9R martensitic transformation of Cu precipitates and the relaxation process of elastic strains in an Fe–Cu alloy, *Philos. Mag. A*, 80(2000), No. 3, p. 711.

[15] T.H. Lee, Y.O. Kim, and S.J. Kim, Crystallographic model for bcc-to-9R martensitic transformation of Cu precipitates in ferritic steel, *Philos. Mag.*, 87(2007), No. 2, p. 209.

[16] G. Han, Z.J. Xie, Z.Y. Li, B. Lei, C.J. Shang, and R.D.K. Misra, Evolution of crystal structure of Cu precipitates in a low carbon steel, *Mater. Des.*, 135(2017), p. 92.

[17] H.R. Habibi, Atomic structure of the Cu precipitates in two stages hardening in maraging steel, *Mater. Lett.*, 59(2005), No. 14-15, p. 1824.

[18] J. Wang, H. Zou, C. Li, Y.H. Peng, S.Y. Qiu, and B.L. Shen, The microstructure evolution of type 17-4PH stainless steel during long-term aging at 350°C, *Nucl. Eng. Des.*, 236(2006), No. 24, p. 2531.

[19] S.W. Thompson, Microstructural characterization of an

as-quenched HSLA-100 plate steel via transmission electron microscopy, *Mater. Charact.*, 77(2013), p. 89.

[20] T.J. Headley and J.A. Brooks, A new Bcc-Fcc orientation relationship observed between ferrite and austenite in solidification structures of steels, *Metall. Mater. Trans. A*, 33(2002), No. 1, p. 5.

[21] A. Saha and G.B. Olson, Computer-aided design of transformation toughened blast resistant naval hull steels: Part I, *J. Comput. Aided Mater. Des.*, 14(2007), No. 2, p. 177.

[22] S.S.G. Banadkouki, D. Yu, and D.P. Dunne, Age hardening in a Cu-bearing high strength low alloy steel, *ISIJ Int.*, 36(1996), No. 1, p. 61.

[23] B. Hwang, C.G. Lee, and T.H. Lee, Correlation of microstructure and mechanical properties of thermomechanically processed low-carbon steels containing boron and copper, *Metall. Mater. Trans. A*, 41(2009), No. 1, p. 85.

[24] M. Mujahid, A.K. Lis, C.I. Garcia, and A.J. DeArdo, HSLA-100 steels: Influence of aging heat treatment on microstructure and properties, *J. Mater. Eng. Perform*., 7(1998), No. 2, p. 247.

[25] S. Panwar, D.B. Goel, O.P. Pandey, and K.S. Prasad, Aging of a copper bearing HSLA-100 steel, *Bull. Mater. Sci*., 26(2003), No. 4, p. 441.

[26] A.N. Bhagat, S.K. Pabi, S. Ranganathan, and O.N. Mohanty, Aging behaviour in copper bearing high strength low alloy steels, *ISIJ Int*., 44(2004), No. 1, p. 115.

[27] R. Hamano, The effect of the precipitation of coherent and incoherent precipitates on the ductility and toughness of high-strength steel, *Metall. Trans. A*, 24(1993), No. 1, p. 127.

[28] L. Skoufari-Themistou, D.N. Crowther, and B. Mintz, Strength and impact behaviour of age hardenable copper containing steels, *Mater. Sci. Technol*., 15(1999), No. 9, p. 1069.

[29] NAVSEA Thechnical Publication, *Base Materials for Critical Applications: Requirements for Low Aalloy Steel Plate, Forgings, Castings, Shapes, Bars, and Heads of HY-80/100/130 and HSLA-80/100*, T9074-BD-GIB-010/0300 (REV. 2), 2012.

[30] W.S. Li, H.Y. Gao, Z.Y. Li, H. Nakashima, S. Hata, and W.H. Tian, Effect of lower bainite/martensite/retained austenite triplex microstructure on the mechanical properties of a low-carbon steel with quenching and partitioning process, *Int. J. Miner. Metall. Mater*., 23(2016), No. 3, p. 303.

[31] D. Isheim, R.P. Kolli, M.E. Fine, and D.N. Seidman, An atom-probe tomographic study of the temporal evolution of the nanostructure of Fe–Cu based high-strength low-carbon steels, *Scripta Mater.*, 55(2006), No. 1, p. 35.

[32] P.K. Ray, R.I. Ganguly, and A.K. Panda, Optimization of mechanical properties of an HSLA-100 steel through control of heat treatment variables, *Mater. Sci. Eng. A*, 346(2003), No.1-2, p. 122.

[33] J.W. Bai, P.P. Liu, Y.M. Zhu, X.M. Li, C.Y. Chi, H.Y. Yu, X.S. Xie, and Q. Zhan, Coherent precipitation of copper in Super304H austenite steel, *Mater. Sci. Eng. A*, 584(2013), p. 57.